Quantitative Experimental Determination of Scattering and Absorption Cross-Section Spectra of Individual Optical Metallic Nanoantennas

Martin Husnik,[1,2,*] Stefan Linden,[2,3] Richard Diehl,[4] Jens Niegemann,[5] Kurt Busch,[6] and Martin Wegener[1,2,†]

[1]*Institut für Angewandte Physik and DFG-Center for Functional Nanostructures (CFN), Karlsruhe Institute of Technology, 76131 Karlsruhe, Germany*

[2]*Institut für Nanotechnologie, Karlsruhe Institute of Technology, 76344 Eggenstein-Leopoldshafen, Germany*

[3]*Physikalisches Institut, Universität Bonn, 53115 Bonn, Germany*

[4]*Institut für Theoretische Festkörperphysik and DFG-Center for Functional Nanostructures (CFN), Karlsruhe Institute of Technology, 76131 Karlsruhe, Germany*

[5]*Laboratory for Electromagnetic Fields and Microwave Electronics, Swiss Federal Institute of Technology (ETH), 8009 Zürich, Switzerland*

[6]*Humboldt-Universität zu Berlin, Institut für Physik, AG Theoretische Optik & Photonik, and Max-Born-Institut, 12489 Berlin, Germany*

(Received 6 July 2012; revised manuscript received 7 October 2012; published 4 December 2012)

Antennas convert propagating radiation to localized electromagnetic energy and to heat. To unambiguously separate between these two aspects, one needs to quantitatively determine the antenna scattering and absorption cross-section spectra. By using a spatial modulation technique combined with a common-path interferometer and lithographically fabricated individual gold nanoantennas, we experimentally determine the scattering and absorption cross-section spectra of different optical antennas simultaneously and quantitatively for the first time.

DOI: 10.1103/PhysRevLett.109.233902 PACS numbers: 42.25.Fx, 42.25.Hz, 42.62.Fi, 84.40.Ba

Metallic antennas can be seen as resonant high-frequency electrical circuits which couple to propagating radiation in free space [1–3]. While the antenna capacitance and Faraday inductance scale proportional to the antenna size, the antenna complex Ohmic impedance due to the moving electron gas in the metal scales inversely with size [4]. The plasmonic regime is reached if the kinetic inductance, which is directly connected to the imaginary part of the antenna's complex Ohmic impedance, overwhelms its usual Faraday inductance. Importantly, also the real part, the usual Ohmic resistance, scales inversely with size and leads to pronounced losses at optical frequencies. The Ohmic resistance can even overwhelm the antenna radiation resistance on resonance [1], which mainly depends on the shape but only weakly on the size of the antenna. This trend may be undesired or desired, depending on the application. For example, Ohmic effects in the antenna limit how much of the incident radiation energy can be transferred by a single metallic nanoantenna to an attached single molecule or semiconductor quantum dot (compared to no antenna) [5–7]. Ohmic effects also limit the accessible localized electromagnetic energy density, i.e., the possible local-field enhancement, which is crucial for, e.g., nonlinear optical frequency conversion [8]. In contrast, relatively large Ohmic resistances, equivalent to large absorption cross sections of metallic nanoantennas, may be desirable for applications of nanoantennas in photothermal cancer therapy [9], where ideally all incident propagating radiation should be converted into local heat (equivalent to small scattering cross sections). Furthermore, in cloaked sensors [10], one aims at a small but finite absorption cross section combined with a vanishing scattering cross section.

To experimentally quantify a given individual nanoantenna, it is thus necessary to measure quantitatively the antenna scattering and absorption cross-section spectra. This is equivalent to determining the real and the imaginary part of the antenna's scattering-amplitude spectra [11]. (As usual, the far field in the presence of the antenna is given by the incident field plus the scattered field, which is expressed as the incident one times the dimensionless scattering amplitude X.) Such measurement has not been accomplished so far. Conventional scattering or dark-field spectroscopy is able to routinely determine the shape of the scattering cross-section spectrum, however, usually with arbitrary units [12] and rarely with calibration [13]. Absorption cross sections have been determined via thermal modulation techniques, but again usually with arbitrary units [12] and only very rarely quantitatively [14]. Simultaneous quantitative measurements of scattering and absorption cross-section spectra of individual nanoantennas are elusive. The sum of scattering and absorption cross section, the extinction cross section, has been determined quantitatively [15,16]. However, extinction alone is not satisfactory, as it leaves open what fraction of the incident radiation is converted into heat.

In this Letter, we directly measure the scattering and absorption cross-section spectra of individual optical nanoantennas simultaneously and quantitatively for the first time. We use a sensitive spatial modulation technique combined with a common-path interferometer. Our systematic experiments on various nanoantennas agree well

with corresponding numerical calculations. This technique may thus pave the road for the detailed quantitative routine characterization of individual metallic nanoantennas.

Following previous work [15,16], we use a modulation technique in which the relative position of the laser spot with respect to the sample is harmonically modulated at some frequency f and with some sizable amplitude a. A lock-in amplifier picks up the resulting small modulation of the transmitted light. In contrast to the tight foci of light discussed in Refs. [17,18], we intentionally rather use large foci to ease the analysis and to have well-defined transverse polarizations. Along these lines, we have previously determined quantitatively the extinction cross-section spectra of individual split-ring resonators [16]. To experimentally separate between the contributions of scattering and absorption, one needs additional phase information. This information can be obtained by letting the transmitted wave interfere with a reference wave which is not influenced by the antenna. To avoid mechanical instabilities, we use a common-path interferometer (see Refs. [19–22]) as illustrated in Fig. 1.

In this setup, the light of a supercontinuum laser (Fianium SC450) is spectrally filtered by a tunable monochromator and sent through a single-mode optical fiber to obtain a well-defined spatial profile. A polarizer at the output side ensures well-defined linear polarization, which is turned into circular polarization by a quarter-wave plate. A Wollaston prism splits the two linear contributions into two beams including an angle of 0.25°. Focusing with an aspheric lens (used with an effective numerical aperture of $NA_{eff} = 0.3$) leads to two spatially separated and orthogonally linearly polarized foci of light on the sample.

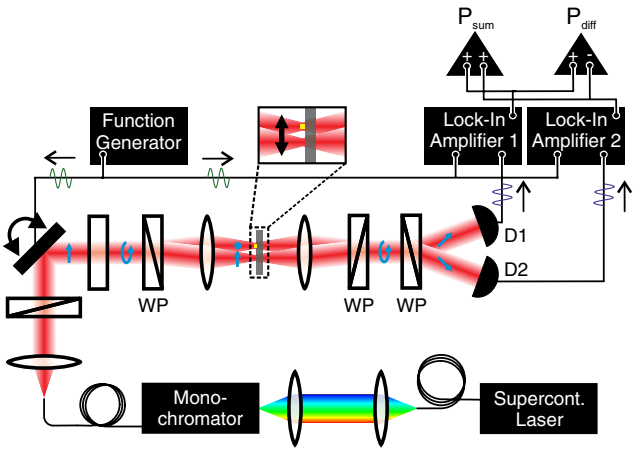

FIG. 1 (color online). Setup for the quantitative measurement of scattering and absorption cross-section spectra of individual metallic nanoantennas. A spatial modulation technique is combined with a common-path interferometer using three Wollaston prisms (WP). For each wavelength, the sum signal (P_{sum}) of the two detectors (D) delivers the sum of scattering and absorption (i.e., the extinction) cross section. Together with the difference signal (P_{diff}) it gives the scattering cross section.

The positions of both foci are modulated along the x direction by a piezocontrolled mirror. Only one focus interacts with the nanoantenna. The other one, which is displaced by 40 μm, serves as the "second arm" of the interferometer. The two contributions transmitted by the sample are collected by a second identical aspheric lens (with NA = 0.5) and are converted into a single generally elliptically polarized beam (circularly polarized beam without antenna) by a second Wollaston prism. A third Wollaston prism separates the two orthogonal linear polarizations oriented 45° with respect to the original incident linear polarization into two beams that are sent onto two identical InGaAs photodetectors connected to identical amplifiers. Our straightforward analysis (for details of the lengthy derivation, see Supplemental Material [23]) shows that the real and imaginary parts of the scattering amplitude in forward direction [11] X for each vacuum wavelength λ are then given by

$$\mathrm{Re}\,(X) = \frac{\pi^2 w_0^2}{\lambda^2}\Sigma_{\mathrm{RDS}}$$

and

$$\mathrm{Im}\,(X) = \frac{\pi^2 w_0^2}{\lambda^2}\Delta_{\mathrm{RDS}}.$$

Here, w_0 is the Gaussian $1/e^2$ intensity radius [24] of the focus (determined by a careful knife-edge measurement in the focal plane). Σ_{RDS} and Δ_{RDS} are the sum and the difference dimensionless relative differential signals (RDS) [23]. This quantitative analysis uses the optical theorem [11]

$$C_{\mathrm{ext}} = \frac{1}{\pi}\lambda^2 \mathrm{Re}(X).$$

For the scattering cross section, we use the expression

$$C_{\mathrm{sca}} = \frac{2}{3\pi}\lambda^2|X|^2 = \frac{2}{3\pi}\lambda^2[\mathrm{Re}^2(X) + \mathrm{Im}^2(X)],$$

which can be derived in the limit of an ideal electric-dipole [11]; i.e., from the multipole expansion of a scatterer only the dipole term is kept. The wavelength-dependent absorption cross section C_{abs} follows from the definition of the extinction cross section

$$C_{\mathrm{ext}}(\lambda) = C_{\mathrm{sca}}(\lambda) + C_{\mathrm{abs}}(\lambda).$$

In principle, provided one knows the relative positions of focus and nanoantenna, a single measurement suffices for each wavelength. In practice, however, we do not have this knowledge. Thus, as previously [16], we raster scan the sample in the xy plane normal to the optical axis. Resulting examples are depicted in Fig. 2. The two-dimensional data sets of the sum channel reveal a positive maximum and a negative minimum of the RDS separated by approximately two times the modulation amplitude a. The size of the two extrema directly reflects the Gaussian spot size; i.e., it

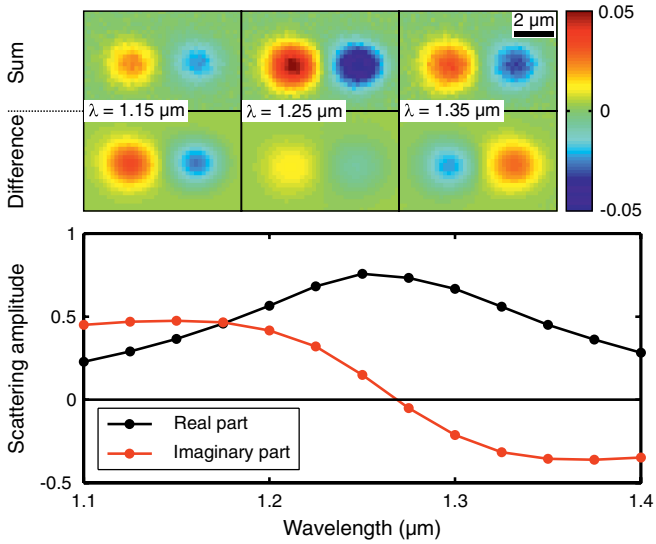

FIG. 2 (color online). Example of a dimensionless scattering-amplitude spectrum $X(\lambda)$ versus vacuum wavelength λ [for the case of the straight dipole antenna shown in Fig. 3 (top)]. Real and imaginary parts of $X(\lambda)$ are shown. Each data point results from a scan in the xy plane (see top). The modulation frequency is $f = 1.2$ kHz and the modulation amplitude is $a = 2.0$ μm. The focus radius changes with wavelength and is typically about $w_0 = 1.55$ μm.

reflects w_0 (which may change with wavelength). The positive maximum results from starting the modulation with the focus on the nanoantenna. Upon moving it away, the transmitted signal increases, corresponding to a positive RDS. Conversely, we get a negative RDS if the modulation starts away from the nanoantenna. Fitting to these data enhances the signal-to-noise ratio and provides an independent cross-check for the modulation amplitude as well as for the value of w_0, which directly enters into the quantitative cross sections. The difference RDS channel exhibits a similar behavior in the xy plane, but the sign (i.e., maximum or minimum) depends on the phase of the scattered wave.

Such a modulated common-path interferometer turns out to be extremely sensitive. For example, scanning over a clean optical-grade glass substrate without any nanoantennas, we observe reproducible yet spatially wildly fluctuating relative differential signals on the order of 1% for the difference channel (not depicted). These parasitic signals are due to few-nanometer-scale roughness of the glass surface, leading to appreciable phase shifts between the two foci on the sample. Comparable signals are indeed expected from our individual nanoantennas. This means that our nanoantenna experiments require essentially nearly atomically flat substrates. We choose free-standing 30 nm thin SiN membranes with 100 μm $\times$ 100 μm footprint (Silson, Ltd.), supported by a macroscopic Si substrate on the sides. This geometry corresponds to that used in our early electron-energy-loss-spectroscopy experiments on split-ring resonators (SRR) [25]. For these substrates, we measure negligible RDS in the difference channel without nanoantennas. These substrates also largely eliminate the asymmetry of usual half-space geometries for thick substrates. All our nanoantennas have been made by standard electron-beam lithography, high-vacuum electron-beam evaporation of gold, and a lift-off procedure.

Next, we apply this quantitative single-antenna technique to two groups of examples. In the first group, we study the transition from a straight gold dipole nanoantenna to a SRR [26]. In essence, this means that we take a straight metal wire of nearly fixed length and bend it into an almost closed ring. It is known that this transition does not affect the resonance wavelength too much, allowing for a direct comparison. Considering a snapshot of the charge distribution oscillating with the frequency of light, the electric-dipole moment of the nanoantenna is proportional to the separation between positive and negative charges at the two wires' ends. Clearly, the dipole moment for the straight dipole antenna is thus much larger than that for the SRR. As a result, we expect the resonant scattering cross section of the straight dipole antenna, which scales like the square of the dipole moment, to be larger than for the SRR. Equivalently, we can say that the radiation resistance is larger for the dipole antenna than for the SRR. In contrast, as the wire lengths are nearly the same, the Ohmic resistances of dipole antenna and SRR are similar, equivalent to comparable resonant absorption cross sections.

The insets in Fig. 3 show a corresponding sequence of electron micrographs of individual nanoantennas, all with 35 nm thin gold films. The left column of Fig. 3 also exhibits the measured extinction (black dots) and scattering cross-section spectra (green dots). These data are fairly well described by Lorentzian fits (solid curves), which also serve as guides to the eye. In each case, the difference of extinction and scattering cross-section spectrum delivers the absorption cross-section spectrum (red).

Let us start our discussion with the case of the straight dipole antenna in Fig. 3 (top). For illustration, the corresponding scattering-amplitude spectrum is shown in Fig. 2. For this antenna, the resonant scattering cross section is about half of that of the resonant extinction cross section. In other words, absorption and scattering are roughly similar in magnitude. When making the transition to the SRR, the resonant absorption cross section drops only slightly, whereas the resonant scattering cross section decreases substantially. For example, in the case of the SRR, the resonant scattering cross section is only one fourth of the resonant extinction cross section or, equivalently, only one third of the resonant absorption cross section. Consequently, the resonant extinction cross section is much lower for the SRR than for the straight dipole antenna. The corresponding smaller radiation resistance for the SRR also leads to a smaller overall linewidth.

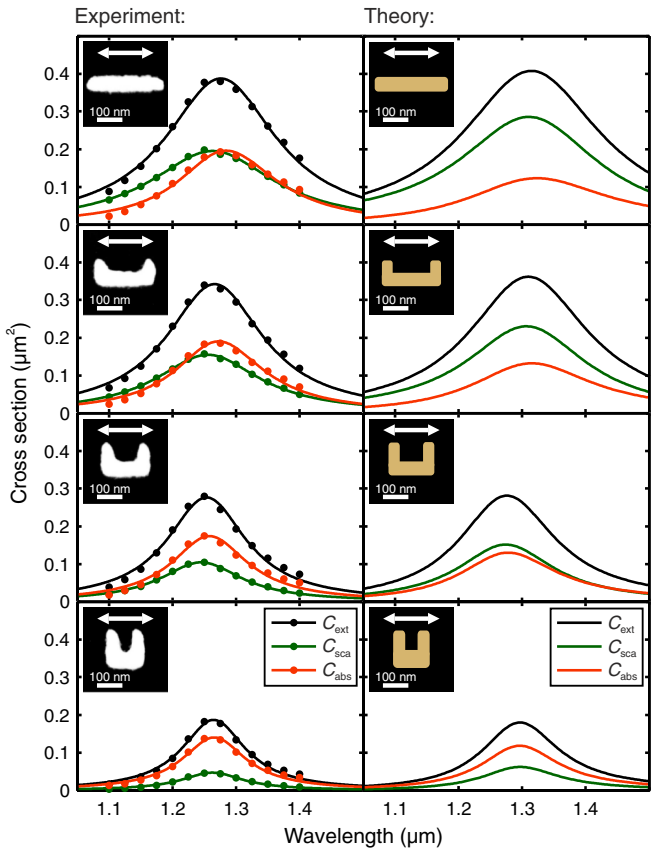

FIG. 3 (color online). First group of examples. Transition from a straight dipole antenna (top) to a split-ring resonator (bottom). In the left column, the dots show the measured scattering C_{sca}, absorption C_{abs}, and extinction cross-section spectra C_{ext} (see legend). The solid curves result from Lorentzian fits. The insets show electron micrographs of the 35 nm thin gold nanoantennas. For all cases, the incident linear polarization is horizontal (see double arrow). The results of corresponding numerical calculations are depicted in the right column on the same scale and in the same format to allow for direct comparison with experiment.

However, the ratio of resonant scattering to absorption cross section is not only a function of the shape of the nanoantenna, but for fixed shape also dependent on the Ohmic resistance. It is this aspect that we wish to highlight in the second group of examples depicted in Fig. 4. Here, we focus on the straight dipole antenna. To experimentally vary the Ohmic damping, we fabricate one antenna with a 35 nm thin gold film and another with an approximately 10 nm chromium layer underneath a 25 nm thin gold film. Chromium is known to have a much larger damping than gold; i.e., the Ohmic resistance increases with increasing Cr thickness. As a result, the ratio of resonant scattering to absorption cross section decreases quite significantly.

As our experiments cannot be compared to any other reference, we now compare them to theory in order to test our reasoning and to rule out possible artifacts. We use a homebuilt computer program based on the discontinuous Galerkin method [27]. Details are described in the

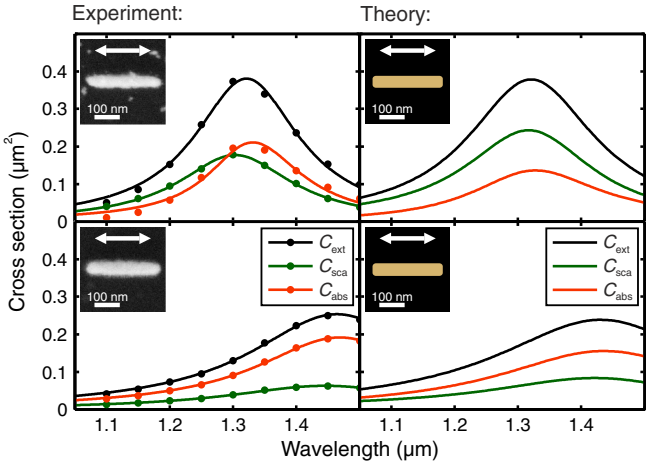

FIG. 4 (color online). Second group of examples. Straight antenna with a 35 nm thin Au layer (top) and with an approximately 10 nm thick Cr layer underneath a 25 nm thin Au layer (bottom) to intentionally increase the antenna damping. The color code of the different curves is as in Fig. 3.

Supplemental Material [23]. The results are depicted in the right-hand-side columns of Figs. 3 and 4. Here we have taken the lateral dimensions (see insets) as well as the gold thickness directly from the experiment. As usual, the gold electric permittivity is described by the free-electron Drude model. We choose an angular plasma frequency of $1.38 \times 10^{16} 1/s$ and a damping (or collision frequency) of $1.88 \times 10^{14} 1/s$. Chromium is described by a Drude-Lorentz model (see Supplemental Material [23]). The 30 nm thin SiN membrane is also accounted for. We choose its refractive index as 2.0. On this basis, we calculate the scattering and absorption cross-section spectra without any further free parameters. The overall agreement with the experimental data in the left column in Figs. 3 and 4 is very good. All qualitative trends discussed above are reproduced and even the absolute cross sections generally match those obtained from the experiment. For the straight dipole antenna, however, we do find somewhat larger scattering cross sections in the numerical simulations compared to the experiment. This deviation might be related to our simple treatment of the metal losses.

Finally, we discuss errors. The statistical errors and day-to-day fluctuations of the cross sections are merely a few percent and could be further improved. Even the reproducibility between similar samples lies in this range (compare the two different Au dipole antennas in Figs. 3 and 4). Systematic errors occur due to the use of the ideal-electric-dipole approximation in the analysis of the experimental data [23]. The comparison with theory (not using this approximation) in Figs. 3 and 4 sets bounds to the systematic errors. These will, however, depend on the type of antenna, its size, and, for a given type and size of antenna, also on wavelength. Thus, for example, our approach could likely not directly be used for a rather large and directional Yagi-Uda type of nanoantenna [28]. In such cases, the

analysis would have to account for higher-order multipole moments depending on the type of antenna under consideration. In contrast, in the limit studied in this Letter, the analysis does *not* depend on the type of antenna to be characterized.

In conclusion, we have applied a quantitative phase-sensitive modulation technique to measure the scattering and absorption cross-section spectra of metallic nanoantennas to two groups of examples: (i) the transition from straight dipole nanoantennas to split-ring resonators and (ii) a variation of the metallic damping for straight dipole nanoantennas. It is our hope that this quantitative technique can be further automated and improved to become a future standard tool for the quantitative characterization of individual metallic nanoantennas.

We thank Andreas Naber for a critical reading of the manuscript. We acknowledge support by the Deutsche Forschungsgemeinschaft (DFG), the State of Baden-Württemberg, and the Karlsruhe Institute of Technology (KIT) through the DFG—Center for Functional Nanostructures (CFN) within Subprojects No. A1.2 and No. A1.5. The project METAMAT is supported by the Bundesministerium für Bildung und Forschung (BMBF). M. H. and R. D. have also received funding by the Karlsruhe School of Optics and Photonics (KSOP).

*martin.husnik@kit.edu
†http://www.aph.kit.edu/wegener/

[1] J. D. Kraus and R. J. Marhefka, *Antennas* (McGraw-Hill, New York, 2003).
[2] L. Novotny and N. van Hulst, Nat. Photonics **5**, 83 (2011).
[3] P. Biagioni, J.-S. Huang, and B. Hecht, Rep. Prog. Phys. **75**, 024402 (2012).
[4] N. Engheta, Science **317**, 1698 (2007).
[5] D. J. Bergman and M. I. Stockman, Phys. Rev. Lett. **90**, 027402 (2003).
[6] M. A. Noginov, G. Zhu, A. M. Belgrave, R. Bakker, V. M. Shalaev, E. E. Narimanov, S. Stout, E. Herz, T. Suteewong, and U. Wiesner, Nature (London) **460**, 1110 (2009).
[7] T. J. Seok, A. Jamshidi, M. Kim, S. Dhuey, A. Lakhani, H. Choo, P. J. Schuck, S. Cabrini, A. M. Schwartzberg, J. Bokor, E. Yablonovitch, and M. C. Wu, Nano Lett. **11**, 2606 (2011).
[8] S. Kim, J. Jin, Y.-J. Kim, I.-Y. Park, Y. Kim, and S.-W. Kim, Nature (London) **453**, 757 (2008).
[9] L. R. Hirsch, R. J. Stafford, J. A. Bankson, S. R. Sershen, B. Rivera, R. E. Price, J. D. Hazle, N. J. Halas, and J. L. West, Proc. Natl. Acad. Sci. U.S.A. **100**, 13549 (2003).
[10] A. Alu and N. Engheta, Phys. Rev. Lett. **102**, 233901 (2009).
[11] C. F. Bohren and D. R. Huffman, *Absorption and Scattering of Light by Small Particles* (Wiley, New York, 1983).
[12] P. Zijlstra and M. Orrit, Rep. Prog. Phys. **74**, 106401 (2011).
[13] A. Tcherniak, J. W. Ha, S. Dominguez-Medina, L. S. Slaughter, and S. Link, Nano Lett. **10**, 1398 (2010).
[14] G. Baffou, P. Bon, J. Savatier, J. Polleux, M. Zhu, M. Merlin, H. Rigneault, and S. Monneret, ACS Nano **6**, 2452 (2012).
[15] A. Arbouet, D. Christofilos, N. Del Fatti, F. Vallée, J. R. Huntzinger, L. Arnaud, P. Billaud, and M. Broyer, Phys. Rev. Lett. **93**, 127401 (2004).
[16] M. Husnik, M. W. Klein, N. Feth, M. König, J. Niegemann, K. Busch, S. Linden, and M. Wegener, Nat. Photonics **2**, 614 (2008).
[17] G. Zumofen, N. M. Mojarad, V. Sandoghdar, and M. Agio, Phys. Rev. Lett. **101**, 180404 (2008).
[18] N. M. Mojarad, V. Sandoghdar, and M. Agio, J. Opt. Soc. Am. B **25**, 651 (2008).
[19] J. S. Batchelder and M. A. Taubenblatt, Appl. Phys. Lett. **55**, 215 (1989).
[20] M. A. Taubenblatt and J. S. Batchelder, Appl. Opt. **30**, 4972 (1991).
[21] Y. Matsuo and K. Sasaki, Jpn. J. Appl. Phys. **40**, 6143 (2001).
[22] P. Stoller, V. Jacobsen, and V. Sandoghdar, Opt. Lett. **31**, 2474 (2006).
[23] See Supplemental Material at http://link.aps.org/supplemental/10.1103/PhysRevLett.109.233902 for detailed information.
[24] L. Novotny and B. Hecht, *Principles of Nano-Optics* (Cambridge University Press, Cambridge, England, 2006).
[25] G. Boudarham, N. Feth, V. Myroshnychenko, S. Linden, J. García de Abajo, M. Wegener, and M. Kociak, Phys. Rev. Lett. **105**, 255501 (2010).
[26] M. G. Nielsen, A. Pors, R. B. Nielsen, A. Boltasseva, O. Albrektsen, and S. I. Bozhevolnyi, Opt. Express **18**, 14 802 (2010).
[27] K. Busch, M. König, and J. Niegemann, Laser Photonics Rev. **5**, 773 (2011).
[28] A. G. Curto, G. Volpe, T. H. Taminiau, M. P. Kreuzer, R. Quidant, and N. F. van Hulst, Science **329**, 930 (2010).